

Longitudinal Monitoring of Glioblastoma Small Extracellular Vesicle Evolution Using a Nanodiagnostic to Detect Emergence of Glioma Stem Cells Driving Recurrent Disease

Zhen Zhang^{1,‡}, Richard J Lobb^{1,‡,*}, Paul Tooney^{2,3,4}, Jing Wang^{1,5}, Rebecca Lane¹, Quan Zhou¹, Xueming Niu¹, Sam Faulkner^{2,3}, Bryan W Day^{6,7,8}, Simon Puttick⁹, Stephen Rose⁹, Mike Fay^{3,10,11}, Matt Trau^{1,12*}

¹Centre for Personalized Nanomedicine, Australian Institute for Bioengineering and Nanotechnology (AIBN), The University of Queensland, Brisbane, QLD 4072, Australia

²School of Biomedical Sciences and Pharmacy, College of Health, Medicine and Wellbeing, University of Newcastle, Newcastle, NSW 2308, Australia

³Mark Hughes Foundation Centre for Brain Cancer Research, University of Newcastle, Newcastle, NSW 2308, Australia

⁴Drug Repurposing and Medicines Research Program, Hunter Medical Research Institute, New Lambton Heights, Newcastle, NSW 2305, Australia

⁵Key Laboratory of OptoElectronic Science and Technology for Medicine, Ministry of Education, Fujian Provincial Key Laboratory for Photonics Technology, Fujian Normal University, Fuzhou 350007, China.

⁶Cancer Research Department, QIMR Berghofer Medical Research Institute, Sid Faithfull Brain Cancer Laboratory, Brisbane, QLD 4006, Australia.

⁷School of Biomedical Sciences, The University of Queensland, Brisbane, QLD 4072, Australia.

⁸School of Biomedical Sciences, Faculty of Health, Queensland University of Technology, Brisbane, QLD 4059, Australia.

⁹AdvanCell Isotopes Pty Ltd, Queensland Centre for Advanced Technologies, Brisbane, QLD 4069, Australia

¹⁰School of Medicine and Public Health, College of Health, Medicine and Wellbeing, University of Newcastle, Newcastle, NSW 2308, Australia

¹¹GenesisCare, Lake Macquarie Private Hospital, Newcastle, NSW 2290, Australia

¹²School of Chemistry and Molecular Biosciences, The University of Queensland, Brisbane, QLD
4072, Australia

‡ These authors contributed equally to this work.

* Corresponding authors: Richard Lobb: richard.lobb@uq.edu.au; Matt Trau m.trau@uq.edu.au

Abstract

Assessing therapeutic response in glioblastoma (GBM) is a major factor limiting the clinical development of new and effective therapies. The intracranial location limits serial biopsies, and only provides an intermittent view of the tumor molecular profile from the initial resection. Liquid biopsy techniques, specifically small extracellular vesicle (sEV) analysis, have the potential to overcome these limitations by providing a window into the brain using peripheral blood. To address the need for monitoring tumor evolution and therapeutic resistance, we developed a GBM biomarker panel (ATP1B2, EAAT2, CD24, CD44, CD133 and EGFR) for multiplexed profiling of sEVs using an advanced GBM Extracellular vesicle Monitoring Phenotypic Analyzer Chip (GEMPAC). We successfully tracked patient response to treatment by monitoring changes in glioma stem cell markers on circulating sEVs. We propose that these results provide a strong rationale for using GBM sEVs as a serial monitoring tool in the future clinical management of GBM patients.

1 INTRODUCTION

2 Glioblastoma (GBM) is an aggressive and invasive primary brain tumor originating in the central
3 nervous system (CNS).[1-4] The prognosis of GBM is very poor, with a median survival time of
4 approximately 14 months.[5] The rapid development of treatment resistance and frequent local
5 recurrence are key features contributing to poor patient outcomes.[1, 2, 4] Accurate monitoring of
6 GBM tumor progression is difficult and expensive; depending on imaging modalities, such as
7 magnetic resonance imaging (MRI).[6] The standard diagnostic methods in GBM management
8 (i.e. histopathology of the resection specimens) provide a limited temporal molecular profile of the
9 tumor and are unable to monitor tumor progression dynamically.[7] In addition, detecting early
10 signs of tumor progression is challenging when using MRI, as the interpretation of diagnostic
11 results may be complicated by pseudo-progression after diagnosis (in the first three months after
12 radiotherapy), and by radiation necrosis (3-12 months after radiotherapy).[8, 9] Therefore,
13 developing non-invasive methods for monitoring of tumor evolution during therapy is essential to
14 navigating treatment management in this aggressive disease.

15 In recent years, liquid biopsy has emerged as a diagnostic concept that characterizes and monitors
16 tumor signatures in patient blood for tumor subtyping, prognosis monitoring, and assessing
17 treatment response.[10, 11] These non-invasive approaches can provide a view of the molecular
18 landscape of tumors from blood samples.[12] As a liquid biopsy marker, exosomes or small
19 extracellular vesicles (sEVs) are nano-sized vesicles (50-150 nm) released from cells.[7, 13, 14]
20 These vesicles are critical mediators of cell-cell communication and carry molecular cargo,
21 including proteins, nucleic acids, metabolites, and lipids.[7, 13] Most critically, several studies
22 have indicated that sEVs released by GBM tumors can cross the intact blood-brain barrier (BBB)
23 and gain access to the peripheral blood.[15-18] Several studies have reported an overall increase
24 in bulk sEV concentration in GBM patients relative to healthy controls, with sEV load apparently
25 decreasing following successful treatment of the primary tumor.[7, 15, 19, 20] Other studies,
26 however, have suggested that systemic increases in bulk sEV concentration are not a GBM-
27 specific phenomenon, meaning sEV concentration alone is unlikely to be a useful metric.[21, 22]
28 Further work has demonstrated that sEVs may reflect the molecular profile of the GBM primary
29 tumor and provide clinical information to direct treatment in a timely manner[23], thereby
30 providing an opportunity to utilize GBM sEVs as a tool to inform clinical management decisions.

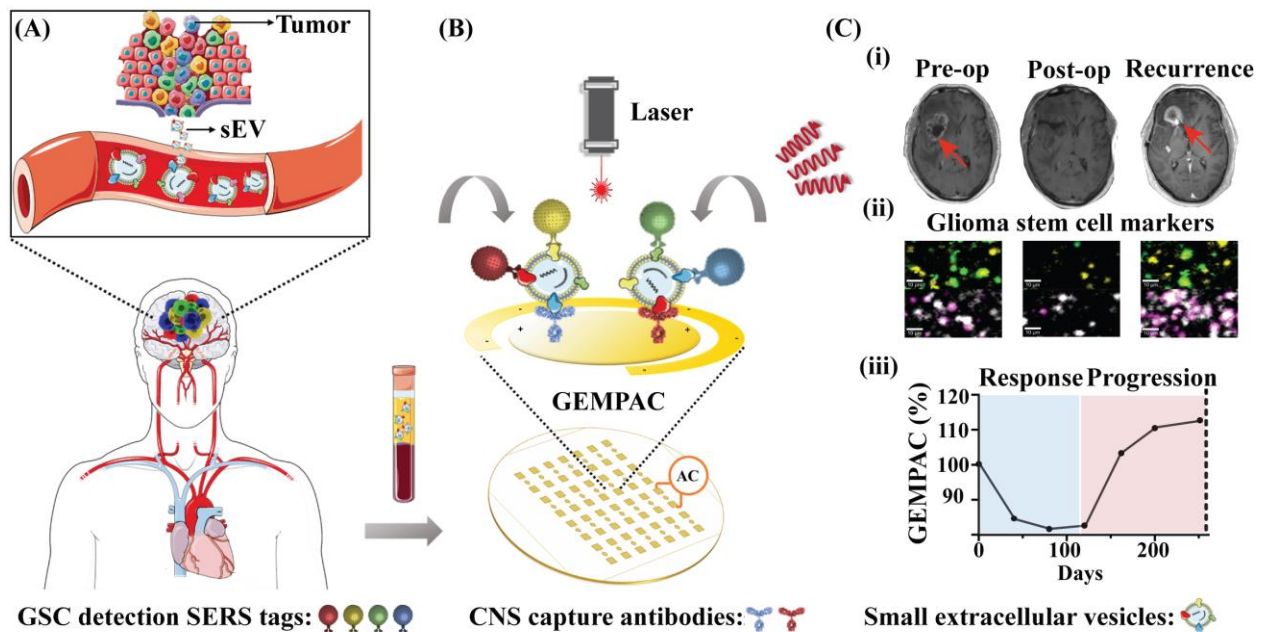
31 Progress in utilizing GBM sEVs has been limited by the challenge of specifically isolating and
32 characterizing GBM sEVs from non-target bulk sEVs in blood. Previous work has attempted to
33 identify specific protein cargo associated with circulating GBM sEVs, including transmembrane
34 L1 cell adhesion molecule,[24] epidermal growth factor receptor variant III (EGFRVIII) [23], von
35 Willebrand factor [20] and syndecan-1.[25] However, these biomarkers are also expressed in a
36 variety of normal tissues and are unable to specifically isolate GBM sEVs.[24, 26, 27] To address
37 the lack of specificity for interrogating sEVs derived from GBM tissue, we identified a unique
38 GBM signature on sEVs in blood. By integrating a GBM sEV signature with a nanoshearing
39 multiplex surface-enhanced Raman spectroscopy (SERS) platform, termed GBM EV Monitoring
40 Phenotypic Analyzer Chip (GEMPAC), we have developed the capability to sensitively profiling
41 the surface protein composition of sEVs in GBM patients with high precision.

42 In the study, the GEMPAC assay precisely captures GBM sEVs by targeting our unique CNS
43 signature composed of transmembrane proteins sodium/potassium-transporting ATPase subunit
44 beta-2 (ATP1B2) and excitatory amino acid transporter 2 (EAAT2), both of which are highly
45 expressed in both normal CNS and GBM tissue.[28-30] The malignant phenotype of captured CNS
46 sEVs were profiled by measuring glioma stem cell (GSC) markers to detect the emergence of GSC
47 subpopulations that could potentially drive recurrent disease and therapy resistance.[31] Previous
48 single-cell RNA sequencing data has revealed certain surface markers that characterize cell-like
49 states of GSCs. In particular, CD24 expression is enriched in neural progenitor cell-like (NPC-
50 like) cells, CD44 in mesenchymal cell-like (MES-like) cells, CD133 in oligodendrocyte-
51 progenitor cell-like (OPC-like) cells, and EGFR in astrocyte-like (AC-like) cells. [32, 33] Using
52 our GEMPAC platform we captured GBM sEVs and monitored GSC subpopulation evolution in
53 patients before and during therapy. Encouragingly, by analyzing GSC subpopulation evolution
54 during therapy, we detected treatment response and tumor progression, thereby opening a new
55 window to facilitate clinical management of GBM. We believe that our diagnostic platform has
56 the potential to facilitate future therapies through monitoring circulating GBM GSC-related sEVs
57 to improve clinical decision-making and therefore patient survival.

59 RESULTS

60 GEMPAC chip dynamically monitors GBM sEV profiles

61 To accurately monitor GBM progression, we hypothesized that circulating sEVs derived from the
62 blood of GBM patients carry specific protein profiles that indicate the degree of tumor burden/or
63 progression in the CNS (Figure 1A). Specifically, we designed a panel of six surface proteins
64 capable of capturing CNS-derived sEVs and monitoring GBM by detecting GSC biomarker
65 expression (Figure 1B). We synthesized unique SERS nanotags conjugated with antibodies
66 targeting GSC surface proteins and dedicated Raman molecule reporters on gold nanoparticles
67 bearing distinct SERS signatures indicating GSC protein expression (Supplementary, Figure S1).
68 The sum of GSC protein expression was defined as the GEMPAC score and used to evaluate
69 disease progression (Figure 1C). Using this multiplexed approach, we combined these biomarkers
70 and investigated their capability as a dynamic monitoring tool of GBM in the blood, including
71 monitoring therapy response and detecting tumor progression for improved clinical management
72 (Figure 1C).

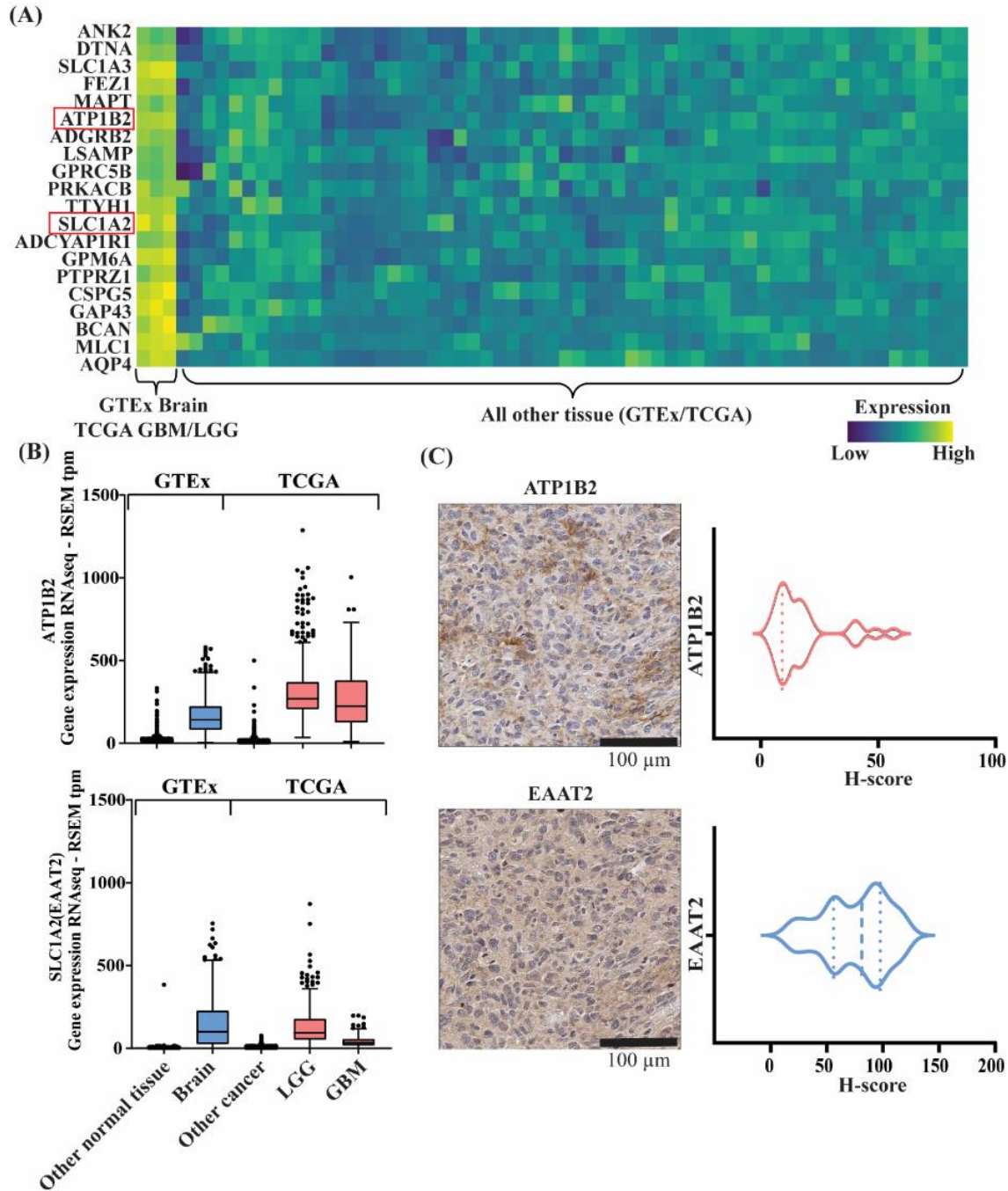


74 **Fig. 1. Multiplexed detection of GBM sEVs by the GEMPAC.** (A) GBM tumor cells release
75 sEVs into the bloodstream. GBM sEVs cross the BBB into the peripheral circulation. (B) GBM

76 sEVs are purified from blood and enriched using GEMPAC functionalized with CNS capture
77 antibodies for selective capture of CNS sEVs. The GEMPAC platform utilizes an alternating
78 current electro-hydrodynamically (AC-EHD)-induced nanoshearing strategy to minimize
79 nonspecific interactions[34] and improve specific capture of CNS sEVs. After that, SERS nanotags
80 that are conjugated with Raman reporters and detection antibodies are applied to the system for
81 multiplex readout. The SERS nanotags with special Raman molecules include, 5,5'-dithiobis (2-
82 nitrobenzoic) (DTNB) (red), 4-Mercaptobenzoic acid (MBA) (blue), 4-mercaptopyridine (MPY)
83 (yellow) and 2,3,5,6-tetrafluoro-MBA (TFMBA) (green). (C) (i) Representative MRI images for
84 tumor scan tumor at pre-operation (pre-op), post-operation (post-op), and recurrence. (ii)
85 Representative pseudo-colored SERS images indicate the presence of each GSC marker in sEVs.
86 (iii) The changes of GSC score on GBM sEVs in response to the treatment and disease progression.
87 The figure was partly generated using Servier Medical Art.

88 **Biomarker selection and validation**

89 To capture GBM sEVs in peripheral blood, targeting CNS-related cell surface markers in sEVs is
90 an essential component of this study. CNS markers were selected through bioinformatic analysis
91 of the Genotype-Tissue expression (GTEx) and The Cancer Genome Atlas (TCGA) databases,
92 with cross-reference to all annotated membrane proteins in the UniProt database. Utilizing this
93 approach, we developed a candidate list of membrane protein-coding genes (Figure 2A;
94 Supplementary, Figure S2 – complete heatmap) of which we selected ATP1B2, the β 2 subunit of
95 Na (+)/K (+) – ATPase expressed on glial cells[29], and solute carrier family 1 member 2
96 (SLC1A2), the astrocyte glutamate transporter EAAT2 for further analysis. [35, 36] These markers
97 were selected based on the suitability of appropriate antibodies targeting extracellular membrane
98 domains. Importantly, the RNA expression levels of ATP1B2 and EAAT2 are highly expressed in
99 brain tissue as well as low grade glioma (LGG) and high-grade GBM, compared to other normal
100 tissues and cancers (Figure 2B; Supplementary, Figure S3). Given the hypothesis that sEVs
101 represent their cell-of-origin[23, 37], this differential expression underpins our approach to capture
102 limited GBM sEVs circulating in the blood.



103

104 **Fig. 2. CNS marker selection and validation.** (A) Heatmap of top 20 CNS markers' RNA
105 expression in TCGA and GTEx RNA-seq databases. Low expression is indicated in blue and high
106 expression is indicated in yellow. (B) Tukey's boxplot indicating *ATP1B2* and *SLC1A2* (EAAT2)
107 genes are highly expressed in normal brain and brain tumor tissues (GBM and low-grade gliomas,
108 LGG) in TCGA and GTEx RNA-seq databases. (C) Primary GBM tumors (n = 31) were labeled

109 for ATP1B2 and EAAT2. Violin plots show the H-score labeling intensity across the cohort. Scale
110 bar = 100 μ m.

111 We then clinically validated our bioinformatic selection of ATP1B2, EAAT2 through IHC of
112 primary GBM tissues. For ATP1B2, low-intensity labeling reflected in low H-scores (mean 17.58
113 +/- 13.42; range 3.96 - 56.53) was detected across the cohort of tumors (Figure 2C). ATP1B2
114 labeling was observed diffusely spread throughout the dense neuropil, which normally contains
115 the nerve fibers and synapses and glial processes (Figure 2C). The labeling of ATP1B2 on control
116 tissues was also analyzed, in which strong ATP1B2 labeling of the cell membrane and cytoplasm
117 of photoreceptor cells; cells of the inner nuclear layer of the human retina; and positive labeling of
118 neuropil in human cortex (Supplementary, Figure S4A & B). Moderate EAAT2 labeling was
119 detected in tumor tissue for all cases of GBM (mean 75.89 +/- 28.88; range 18.13 – 119.69; Figure
120 2C). EAAT2 labeling was detected diffusely throughout the neuropil across the tumor sections
121 with occasional intense labeling of cell membranes and processes (Figure 2C). In the control
122 tissues, no EAAT2 expression were present in colonic crypts but in the human brain cortex strong
123 EAAT2 labeling was observed in astrocytes (Supplementary, Figure S4C & D).

124 After validating the selection of CNS markers, CD24, CD44, CD133 and EGFR were selected to
125 monitor different cell-like states of GSCs.[31] Specifically, scRNA-seq data has revealed that
126 CD24 is enriched in NPC-like GSCs, CD44 in MES-like GSCs, CD133 in OPC-like GSCs, and
127 EGFR is enriched in AC-like GSCs.[32, 38, 39] These surface GSC markers correlate with an
128 aggressive phenotype, poor survival, and associated with the rapid development of treatment
129 resistance.[31, 40-48] Transcriptomic expression based on the TCGA dataset confirmed that all
130 these markers are expressed in GBM (Supplementary, Figure S5). We then validated the
131 expression of CD44, CD133 and EGFR in GBM tumor tissues through IHC labeling
132 (Supplementary, Figure S4 & S6). EGFR (mean 173.01 ± 54.25 ; range 2.65 – 259.59) and CD44
133 (mean 130.58 ± 43.84 ; range 57.66 – 205.24) were highly expressed across all the tumor tissues
134 with intense labeling of tumor cell membranes. Minimal labeling was detected in most GBM tumor
135 sections for CD133 (mean 0.26 ± 0.80 ; range 0 – 4.20), with occasional positive labeling detected
136 sparsely throughout the tumor (Supplementary, Figure S6).[45] IHC labelling for CD24 was not
137 completed across the cohort of tumor tissues in this study, as the labelling of the cells and tissue
138 structures within the control tissues with several antibodies was not consistent with that reported

139 in the Human Protein Atlas. However, we chose to continue with CD24 in this study due to the
140 protein expression of GBM tissue in the Human Protein Atlas. Given the expression of these
141 biomarkers in GBM tissues based on TCGA dataset and IHC results, measuring the expression
142 changes of CD24, CD44, CD133 and EGFR on CNS derived sEVs from the same GBM patients
143 may help predict and track disease progression and treatment response.

144 **Single nanoparticle analysis and GEMPAC marker validation**

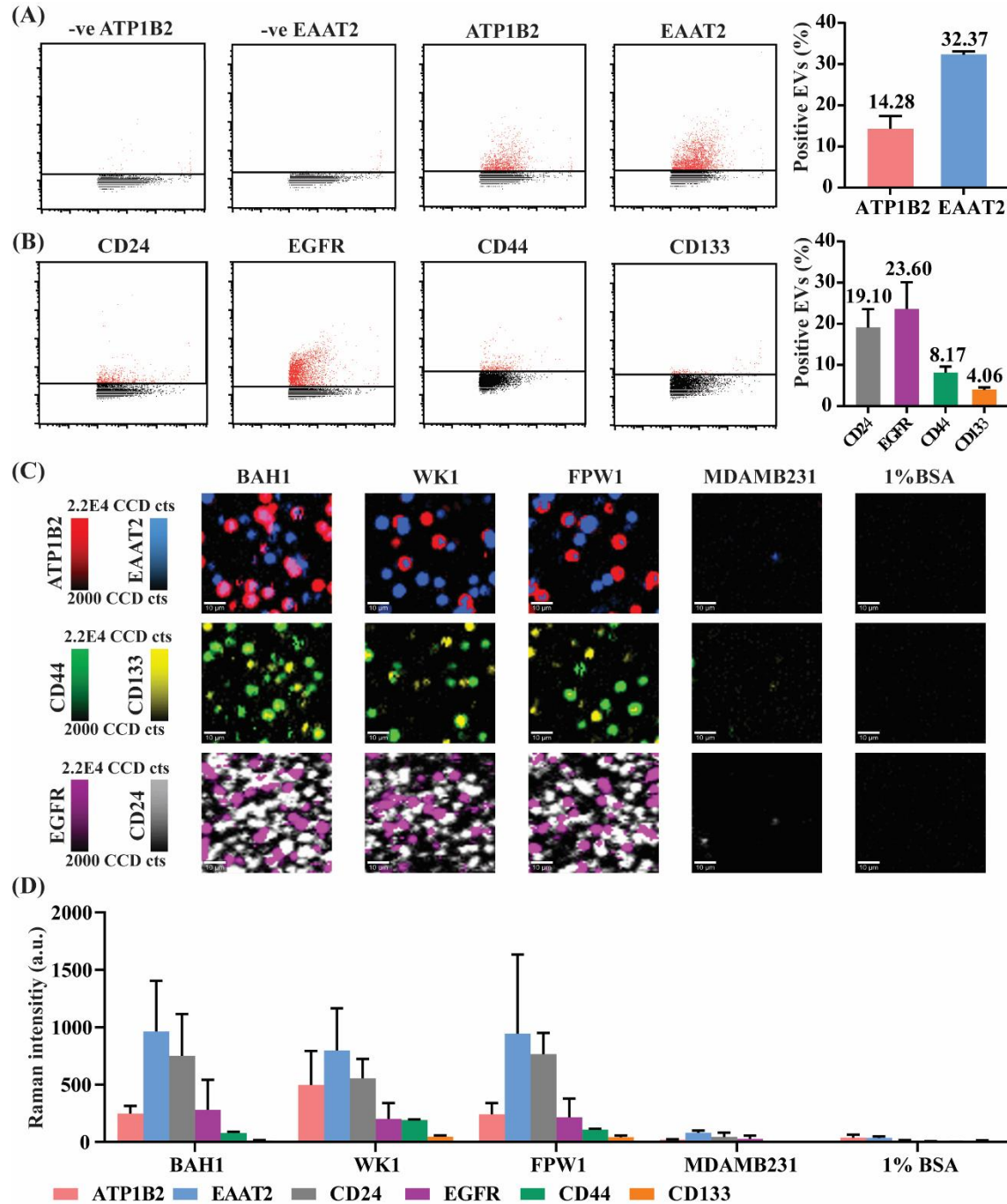
145 We then sought to validate our hypothesis that ATP1B2 and EAAT2 are specifically enriched on
146 the surface of GBM sEVs. To establish an *in vitro* model for GBM sEV analysis, the expression
147 of ATP1B2 and EAAT2 in three unique patient-derived GBM cell lines (BAH1, WK1, and FPW1;
148 representing classical or mesenchymal GBM subtypes[49]) were validated using flow cytometry.
149 In support of our bioinformatic selection of CNS candidates and IHC results, ATP1B2 and EAAT2
150 were highly expressed on the cell surface of three patient-derived GBM cell lines (Supplementary,
151 Figure S3C & D), and therefore as a result have the potential to be present on the surface of GBM
152 sEVs.

153 Next, we collected sEVs from our GBM patient-derived cell line panels and purified them through
154 size exclusion chromatography (SEC).[50] Purified sEVs were characterized by nanoparticle
155 tracking analysis (NTA), showing a characteristic modal size of 90-100 nm (Supplementary,
156 Figure S7A). We then used transmission electron microscopy (TEM) to visualize the morphology
157 of purified sEVs (Supplementary, Figure S7B). Following this, the surface expression of the
158 canonical sEV tetraspanin CD9 and CD63 were measured by nanoflow cytometry (nanoFCM)
159 (Supplementary, Figure S7C), and western blot demonstrated the presence of internal HSP70 and
160 absence of the endoplasmic reticulum-associated molecular chaperone, calnexin (Supplementary,
161 Figure S7D).

162 We next evaluated if the expression of ATP1B2 and EAAT2 was specifically enriched on GBM
163 sEVs. As we hypothesized, cell-of-origin-specific enrichment of ATP1B2 and EAAT2 were
164 detected on GBM sEVs (14.22% and 32.37% respectively), while MDA-MB-231-derived breast
165 cancer sEVs (-ve) contained negligible levels of both CNS markers (Figure 3A; Supplementary,
166 Figure S8). Next, we evaluated the expression of the GSC markers CD24, CD44, CD133, and

167 EGFR on the surface of GBM sEVs. Using single nanoparticle analysis by nanoFCM, we found
168 high levels of CD24 (19.1%) and EGFR (23.6%), moderate levels of CD44 (8.17%) and low levels
169 of CD133 (4.06%) (Figure 3B; Supplementary, Figure S8).

170 After validating that we have identified a unique CNS signature for the analysis of GBM sEVs,
171 we sought to develop an approach that meets the requirements for sensitive and specific detection
172 of GBM sEVs that is clinically translatable (GEMPAC). We carried out a specificity assay to
173 examine the functionality and specificity of the GEMPAC platform. Each electrode of the
174 GEMPAC was functionalized with dual capture antibodies, anti-ATP1B2 and anti-EAAT2, for
175 capturing GBM sEVs. A purified total of 5×10^8 sEVs particles were then applied to individual
176 electrodes and subsequent AC-EHD nanomixing facilitated specific binding of GBM sEVs while
177 simultaneously reducing non-specific interactions.[34] Following this, unique SERS nanotags
178 were applied to each electrode to detect targeted markers on captured sEVs simultaneously.
179 Pseudo-colored SERS mapping images for GBM sEVs are shown in Figure 3C. High expression
180 of both ATP1B2 and EAAT2 was observed for the GBM cell line-derived sEVs (BAH1, WK1,
181 and FPW1), with minimal signals detected for non-GBM sEVs (MDA-MB-231 breast cancer) and
182 an sEV-free control (Figure 3D). Expression of the putative prognostic GSC markers CD24, CD44,
183 CD133 and EGFR were also detectable in the GBM sEVs and absent from other samples due to
184 the specific capture of GBM sEVs (Figure 3D). As a result, combining these markers could
185 distinguish GBM sEVs from other malignancies.



186

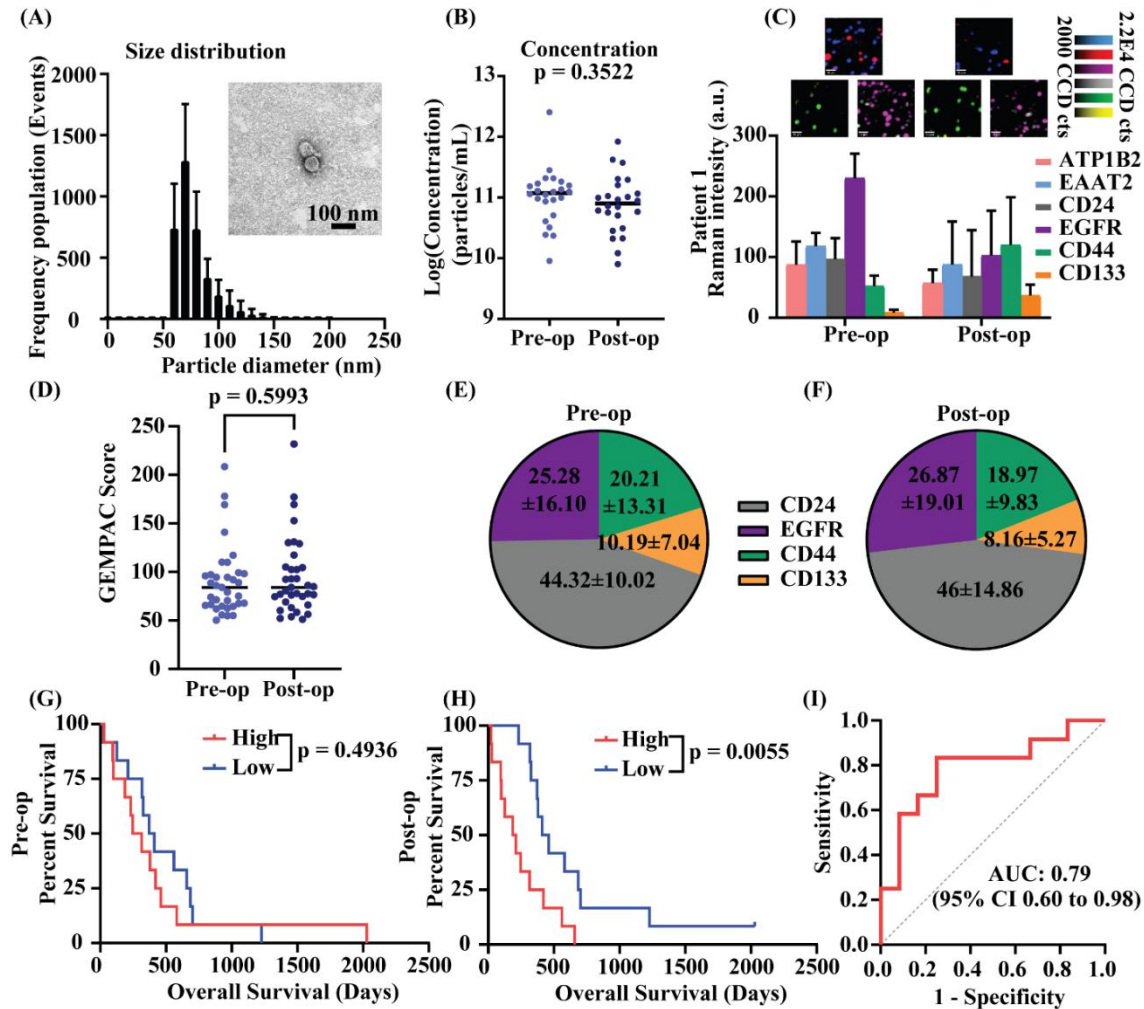
187 **Fig. 3. Expression of selected markers on GBM sEVs by single nanoparticle analysis and**
188 **GEMPAC.** (A) Single nanoparticle analysis by nanoFCM shows the expression of CNS markers
189 (ATP1B2 and EAAT2) in breast cancer cell line MDAMB231 (-ve) and WK1 sEVs. Average
190 histogram measurements are the average expression of 3 GBM cell line sEVs (WK1, BAH1,
191 FPW1). (B) Single nanoparticle analysis by nanoFCM shows the expression of GSC markers

192 (CD24, EGFR, CD44, and CD133) as representative nanoFCM images and average histogram
193 measurements in three GBM cell lines. (C) Representative Raman images for all of marker's
194 detection in GBM cell lines using GEMPAC. Scale bar = 10 μm . (D) Raman intensity
195 measurements of sEVs from each GBM cell line with different SERS nanotags; DTNB-ATP1B2
196 (red), MBA-EAAT2 (blue), TFMBA-CD44 (green), MPY-CD133 (yellow), TFMBA-EGFR
197 (purple) and MPY-CD24 (grey). MDA-MB-231 breast cancer cells and EV-free medium were
198 used as negative controls to show biomarker specificity. Data are represented as mean \pm standard
199 error.

200 **Analysis of GBM patient sEVs sampled before and after surgical resection by GEMPAC**

201 Given the specificity of the GEMPAC assay for analyzing GBM sEVs, we next sought to
202 investigate the composition of GBM sEVs in the blood of GBM patients. Pre- and post-op blood
203 plasma were sourced from GBM patients. sEVs were purified from plasma using SEC and
204 analyzed with TEM and nanoFCM to confirm size distribution and concentration of particles
205 (Figure 4A & B). There were no significant differences in sEV size and concentration at the two
206 time points ($p > 0.05$) (Figure 4B), indicating that these specific sEV properties provide little
207 prognostic or diagnostic information overall. Therefore, our approach of profiling the phenotype
208 of GBM sEVs using GEMPAC may offer more insights for diagnostic and prognostic applications
209 in GBM patients.

210 To address this, we successfully profiled GBM sEVs with our GEMPAC platform by quantifying
211 the composition of ATP1B2, EAAT2, CD24 CD44, CD133, and EGFR (Representative patient,
212 Figure 4C). To understand changes in circulating GBM sEVs, each GSC marker was normalized
213 by the CNS markers (ATP1B2 and EAAT2) and combined into the GEMPAC score to provide
214 insights into the tumor burden of GBM patients. A total of 36 patients were profiled to investigate
215 if the GEMPAC score changed after surgical resection. There was no significant change in the
216 GEMPAC score before and after the surgery ($p > 0.05$) (Figure 4D), and the phenotypic
217 composition of GSC markers on circulating GBM sEVs remained the same (Figure 4E & F).



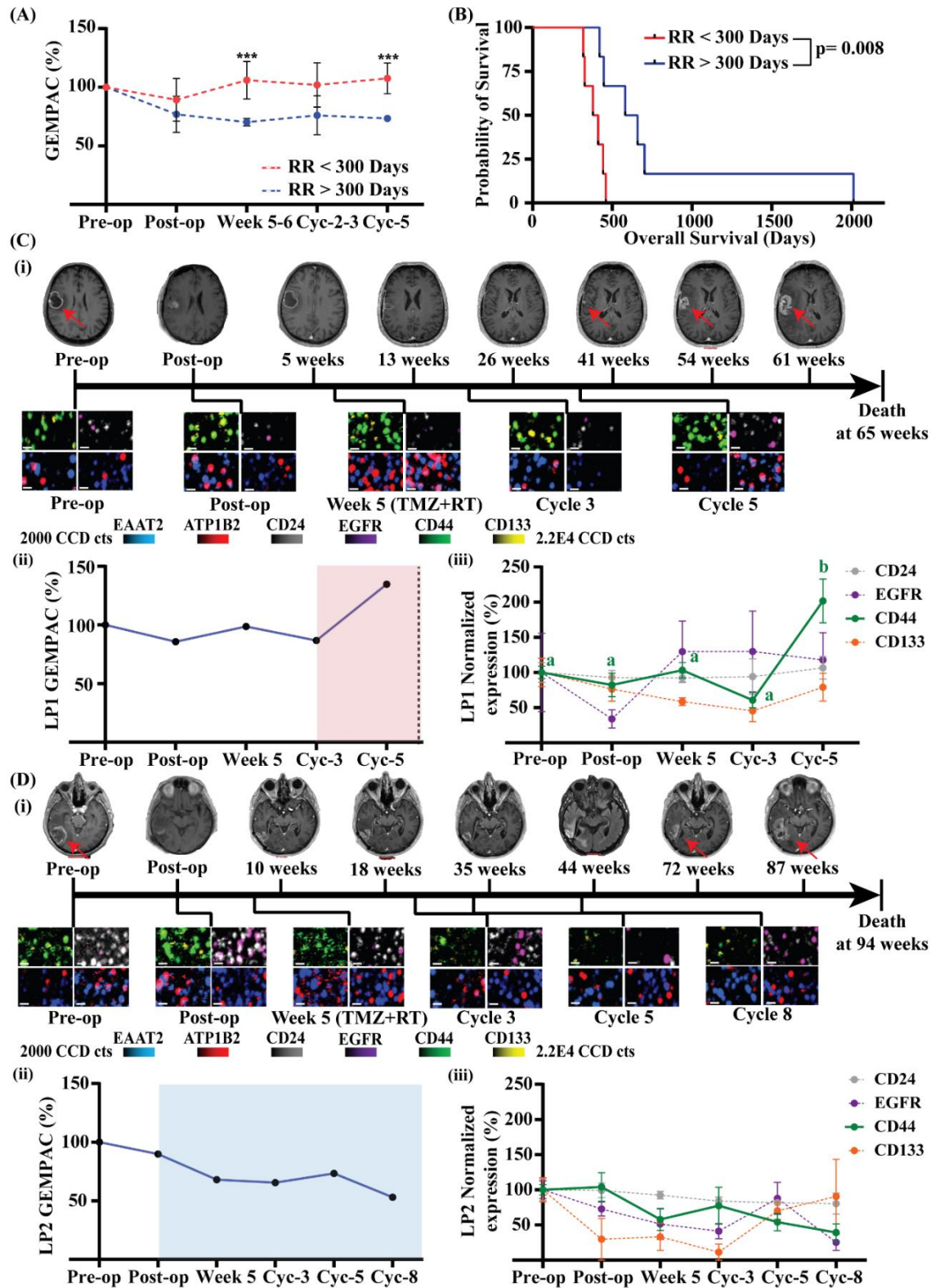
218

219 **Fig. 4. Analysis of sEVs in plasma before and after surgical resection in GBM patients.** (A)
 220 GBM patient samples (n = 36) sEV size distribution. (B) GBM sEV concentration in pre-op and
 221 post-op. (C) Raman intensity measurements of each marker with SERS images in pre-op and post-
 222 op in the representative GBM patient, DTNB-ATP1B2 (red), MBA-EAAT2 (blue), TFMBA-
 223 CD44 (green), MPY-CD133 (yellow), TFMBA-EGFR (purple), and MPY-CD24 (grey). Data are
 224 represented as mean ± standard error (n = 4). (D) All the GBM stem cell markers were normalized
 225 by CNS markers and sum as GEMPAC score. Comparison of GEMPAC score between pre-op and
 226 post-op. The proportion of each normalized GSC marker in (E) pre-op and (F) post-op. Kaplan-
 227 Meier plots of overall survival by GEMPAC score. Survival outcome differences in pre-op (G)
 228 and post-op (H). (I) ROC curve analysis for GEMPAC score between short and long overall
 229 survival groups.

230 Next, we investigated if the GEMPAC score was able to predict overall survival in a cohort of 24
231 patients who received only standard care temozolomide (TMZ) and radiotherapy (RT). Patients
232 were categorized into either high (> median GEMPAC score) or low (< median GEMPAC score)
233 groups. Before surgical resection there was no correlation in overall survival ($p = 0.4936$) (Figure
234 4G), however, after surgical resection, patients with a high GEMPAC score had significantly
235 shorter survival compared to patients with a low GEMPAC score ($p = 0.0055$) (Figure 4H). To
236 investigate the sensitivity and specificity of the GEMPAC score for predicting overall survival, a
237 1-year overall survival was assessed by receiver operating characteristic (ROC) curves. In this
238 context, the area under the curve (AUC) for predicting overall survival after surgical resection
239 (post-op) was 0.79 (95% CI 0.6-0.98) (Figure 4I). These results indicate the GEMPAC score from
240 circulating GBM sEVs could predict patients' survival after surgery, likely reflecting the
241 remaining tumor burden after surgical resection which is a predictor of survival after resection.[51]

242 **Longitudinally monitoring radiological recurrence and sEV evolution by GEMPAC**

243 Our understanding of glioblastoma heterogeneity is limited in terms of the cellular landscape at
244 various stages of disease evolution during standard of care therapies. Clinical progress is restricted
245 due to this limited knowledge of GBM evolution and inability to measure tumor evolution in real-
246 time during therapy. To investigate evolutionary changes during GBM progression, we isolated
247 and profiled GBM sEVs from the plasma of 12 GBM patients with longitudinal blood samples.
248 We subsequently evaluated the relative expression of CNS-related markers ATP1B2, EAAT2, and
249 GSC-related markers CD24, CD44, CD133, and EGFR in sEVs before and during therapy.
250 Furthermore, the expression of ATP1B2, EAAT2, CD44, CD133, and EGFR in primary tumor
251 tissues were confirmed by IHC ($n = 11$) (Supplementary, Figure S9) to confirm that these markers
252 were expressed in the primary tumor. We then evaluated the results of GEMPAC in relation to
253 clinical interpretation of response to treatments in conjunction with MRI and where available with
254 positron emission tomography (PET) scans.



255

256 **Fig. 5. Tracking GSC surface markers on GBM sEVs detects radiological recurrence. (A)**

257 The comparison of GEMPAC score between patients that had radiological recurrence (RR) less

258 than 300 days and more than 300 days. Data are represented as mean \pm standard deviation. *** p
259 < 0.001. (B) Kaplan-Meier plots of overall survival demonstrate MRI detected radiological
260 recurrence is associated with overall survival. (C) Representative longitudinal case showing
261 detection of progression with the GEMPAC analysis before MRI. (i) MRI images and SERS
262 mapping images of LP1. Red arrows indicated tumor location. Scale bar = 10 μ m; (ii) GEMPAC
263 score for LP1 before and during the treatment indicating progression (red area) before MRI
264 detected recurrence at 41 weeks; (iii) Normalized GSC-related protein, CD24 (grey line), CD44
265 (green line), CD133 (yellow line), and EGFR (purple line) composition changes throughout
266 treatment, indicating a significant increase in the MES-like GSC CD44 markers. (Data are
267 represented as mean \pm standard error (n = 4). Significant differences are represented by different
268 letters (p < 0.05). (D) Representative longitudinal case of responding to the TMZ therapy. (i) MRI
269 images and SERS mapping images of LP2. Red arrows indicated tumor location. Scale bar = 10
270 μ m; (ii) GEMPAC score of LP2 before and during the treatment, with the blue area representing
271 a therapeutic response; (iii) Normalized GSC-related protein composition, CD24 (grey line), CD44
272 (green line), CD133 (yellow line), and EGFR (purple line) changes throughout the treatment,
273 indicating a decrease in the MES-like GSC CD44 marker. Data are represented as mean \pm standard
274 error (n = 4).

275 We explored the capabilities of the GEMPAC score in monitoring disease progression or a positive
276 therapeutic response. Interestingly, when we analyzed the GEMPAC score in patients that had
277 radiological recurrence detected by MRI within 300 days, we identified a significantly increased
278 GEMPAC score at 5-6 weeks, and cycle 5 of TMZ treatment (Figure 5A). Importantly, there was
279 no significant difference in the total abundance of CNS-derived sEVs throughout treatment
280 (Supplementary, Figure S10), highlighting the importance of measuring the total GSC stem cell
281 marker expression to detect therapeutic response. Disease progression in these patients detected
282 by MRI was correlated to a significantly reduced overall survival (Figure 5B), indicating that
283 monitoring patients during therapy with the GEMPAC assay could accurately determine
284 therapeutic response.

285 To further explore and characterize heterogeneity and evolution within malignant cell populations,
286 we assessed the relative GSC protein composition of circulating GBM sEVs at all timepoints
287 (Figure 5C & D; Supplementary, Figure S12). We observed changes in the landscape of GSC-

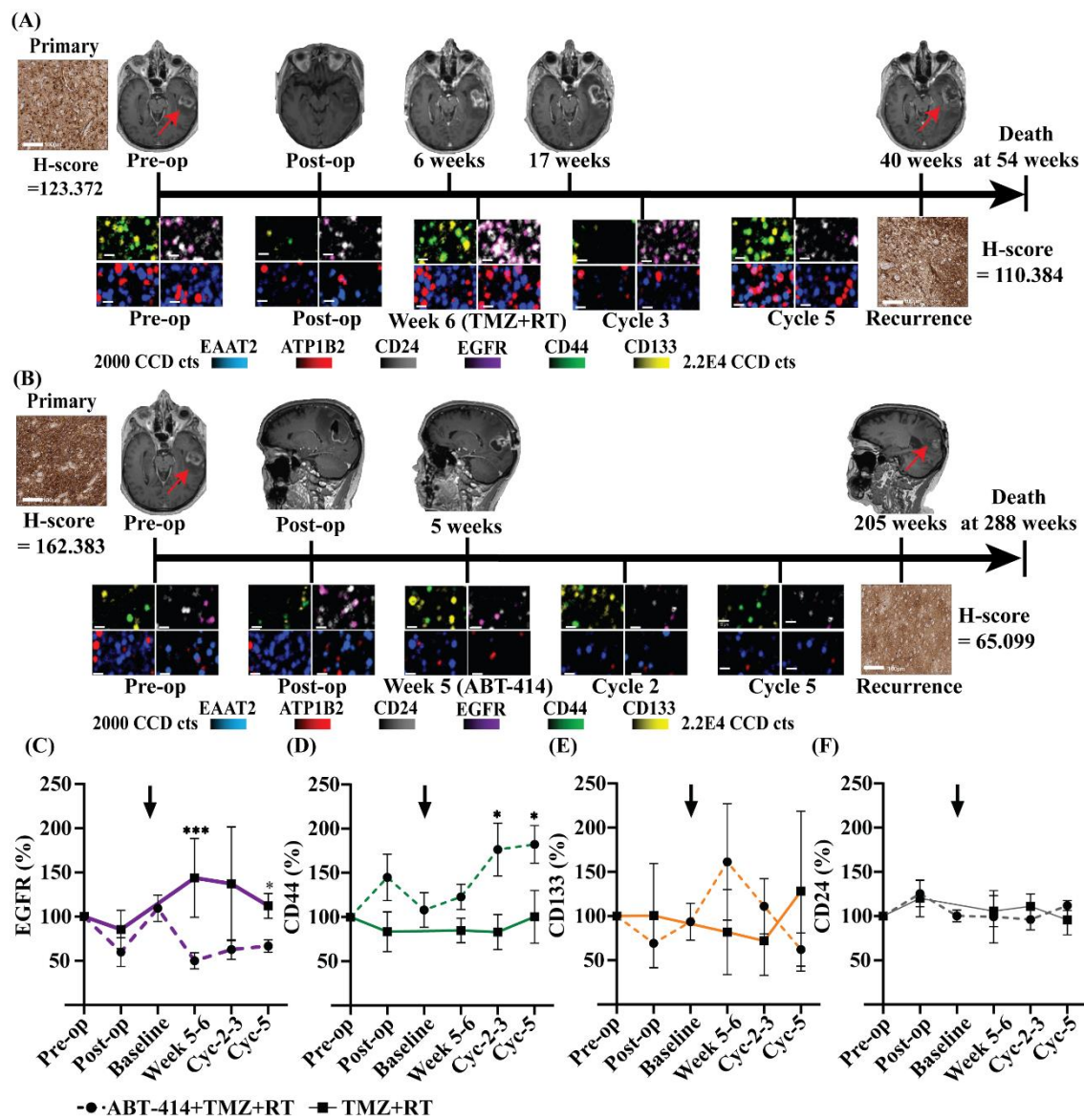
288 related sEV composition at various stages of disease evolution and during TMZ therapy.
289 Specifically, in representative Longitudinal Patient 1 (LP1), MRI indicated tumor debulking and
290 recurrence, and our GEMPAC assay tracked evolutionary changes of GBM sEVs throughout
291 treatment (Figure 5C (i-iii)). In particular, at cycle 5, an elevated GEMPAC score (Figure 5C(i))
292 was driven by a subtle increase in the OPC-like GSC CD133 and a significant increase in the MES-
293 like CD44 GSC marker (Figure 5C(iii)) before radiological recurrence was detected at 41 weeks,
294 suggesting disease progression is driven by a clinically relevant glioblastoma stem cell
295 subpopulation consistent with previous studies.[43, 45, 52] Similarly, multiple patients (LP3, 5-7)
296 also exhibited similar evolutionary changes in circulating sEVs with elevated GEMPAC scores
297 being detected in sEVs before MRI indicated tumor progression (Supplementary, Figure S12 &
298 S13).

299 We next wanted to assess if our GEMPAC assay could monitor positive response to treatment in
300 GBM patients. Our GEMPAC assay detected alterations in the relative expression of CD24, CD44,
301 CD133, and EGFR throughout treatment in representative Longitudinal Patient 2 (LP2) (Figure
302 5D (i-iii)). LP2 responded positively to TMZ+RT which was recapitulated with our GEMPAC
303 assay showing a dynamic reduction in the GEMPAC score from week 5. This was largely driven
304 by reduced levels of the GSC markers CD44 and EGFR. The response our GEMPAC assay
305 detected was further validated with an overall survival of 94 weeks in this patient. Additionally,
306 our GEMPAC assay consistently measured positive response to treatment with RT and TMZ in
307 additional longitudinal patients LP4, 8 & 9 (Supplementary, Figure S12 & S13).

308 **Longitudinally monitoring evolution of GSC-related protein composition of GBM sEVs** 309 **driven by therapy**

310 To directly link the GEMPAC capture and analysis of GBM sEVs to evolutionary changes within
311 the tumor, we compared patients receiving EGFR targeting ABT-414 (depatuxizumab mafodotin)
312 and TMZ+RT (n = 4), versus patients receiving TMZ+RT (n = 5) with matched collection
313 timepoints. Although there was no difference in the GEMPAC score in patients receiving ABT-
314 414 (Supplementary Figure S11), our GEMPAC assay detected evolutionary changes of the tumor
315 through changes in the phenotypic composition of sEVs (Figure 6; Supplementary, Figure S13).
316 In particular, the reduced EGFR expression in a recurrent tumor of a patient treated with ABT-414

317 compared to TMZ+RT alone (Figure 6A & B), correlated with what we observed in our GEMPAC
 318 assay with a significant decrease in EGFR on sEVs (Figure 6C). Due to the molecular and genomic
 319 heterogeneity leading to GBM evolution, various subpopulations of cancer cells with stem-like
 320 properties following radiotherapy and chemotherapy are capable of driving resistance. In this case,
 321 GEMPAC observed a significant increase in the MES-like CD44 GSC marker at cycle 3 and 5 in
 322 patients receiving ABT-414 (Figure 6D). Therefore, although ABT-414 suppressed EGFR
 323 subpopulations, there was limited therapeutic efficacy against mesenchymal subpopulations.



325 **Fig. 6. GEMPAC assay tracks tumor evolution by GSC protein composition in circulating**
326 **GBM sEVs.** Representative IHC staining of EGFR in primary and recurrent tumors of patients
327 receiving either TMZ+RT (A, LP3) or ABT-414 with TMZ+RT (B, LP4). Red arrow indicates the
328 tumor location. SERS images scale bar = 10 μm . IHC scale bar = 100 μm . (C-F) Each GSC-related
329 protein expression changes throughout treatment shows significant knockdown of EGFR and
330 increase of CD44 expression in circulating GBM sEVs. * $p < 0.05$; *** $p < 0.001$. Solid lines are
331 the patients receiving TMZ+RT ($n = 5$) and dotted lines are patients receiving ABT-414 with
332 TMZ+RT ($n = 4$). Data are represented as mean \pm standard deviation. Black arrow indicates when
333 the ABT-414 starts.

334 In addition to our GEMPAC assay measuring treatment efficacy of TMZ+RT, response to the
335 bevacizumab could also be analyzed. Specifically, GEMPAC detected a decrease in GSC markers
336 on circulating sEVs after bevacizumab treatment (Supplementary, Figure S14A). GEMPAC again
337 monitored evolution of the GSC marker composition on GBM sEVs with reduced levels of CD44,
338 CD133 and EGFR at 11 weeks after the start of bevacizumab treatment (Supplementary, Figure
339 S14B & C). Overall, these results demonstrate that GEMPAC has the potential to monitor GBM
340 evolution and therapeutic response in patients being treated with a range of drugs.

341 **DISCUSSION**

342 In the present study, we developed a nanodiagnostic platform, termed GEMPAC, to provide real-
343 time readout of GBM patients under therapy through analysis of sEVs in blood. A key finding
344 from our work is the identification that sEVs derived from GBM tumor cells can be captured and
345 interrogated in patients. As a result, we were able to monitor the emergence of proliferating GSCs
346 from circulating sEVs to dynamically monitor therapy response and tumor evolution.

347 The complexity and degree of genomic and cellular heterogeneity of high-grade gliomas such as
348 GBM is only recently being fully comprehended.[53] This is due, in large part, to technological
349 advancements in single-cell profiling leading to numerous discoveries regarding tumor
350 heterogeneity and the revelation of cellular states; specifically MES-like, NPC-like, AC-like, and
351 OPC-like within malignant brain tumors.[31, 54] However, clinical progress in GBM management
352 will be limited without sophisticated approaches to monitor tumor evolution and progression

353 throughout treatment cycle.[55, 56]Advancements in this area have been limited due to difficulties
354 in sampling longitudinal surgical biopsies, and therefore can only be addressed through liquid
355 biopsies in combination with highly sensitive analytical techniques. In addition to the high
356 sensitivity, the GEMPAC has further advantages for liquid biopsy testing in GBM patients as the
357 analysis of sEVs only requires small volumes that can be routinely collected and cryopreserved.
358 This makes sample collection feasible particularly for patients that do not have access to MRI, as
359 they can be monitored regularly regardless of geographical distribution.

360 At least three of the cellular states within GBM have the capability of propagating tumors in
361 preclinical models, including MES-like, NPC-like and OPC-like.[31-33] Previous studies have
362 proposed quiescent GSCs with MES properties start proliferating in response to therapy and are a
363 driver of disease recurrence.[56, 57] Although the basis for this is unclear, we were able to observe
364 the emergence of a MES-like signature in GBM sEVs by the elevation of CD44 throughout
365 treatment in patients. This elevated level of CD44 on GBM sEVs was associated with disease
366 progression, suggesting that the MES-like GSCs expansion driving recurrent disease[53, 58], can
367 also be monitored dynamically during therapy with the GEMPAC. Another observation in our
368 study was the emergence of elevated CD133 expression on circulating GBM sEVs in a
369 subpopulation of patients, suggesting the expansion of CD133⁺ GSCs. These findings support the
370 premise that CD133⁺ stem cell expansion, which typically have the highest degree of resistance to
371 TMZ [59], persist throughout treatment and could potentially be responsible for the initiation of
372 tumor recurrence.

373 During our analysis, we did not observe an increase associated with recurrent disease in sEV GSC
374 markers CD24 and EGFR during therapy. Although EGFR is a striking feature of GBM, elevated
375 EGFR expression is associated with tumors with a phenotype dominated by AC-like cells. In terms
376 of EGFR expression in GBM, there is evidence in our data of GBM evolution in response to
377 therapy. In particular, circulating sEVs in patients treated with ABT-414 indicated a shift to a
378 MES-like cellular state with downregulation of EGFR and elevation of CD44, an observation that
379 was seen in the evolutionary changes of the recurrent tumor. There is evidence that a phenotypic
380 shift to a MES phenotype can be driven by multiple factors, including inherent resistance to
381 therapy; a phenotypic shift among individual cells; or changes in the proliferative rates among cell-

382 likes GSC states of GBM.[31, 60] In our study, we were able to observe these changes in real-time
383 as sEVs from MES-like were increasingly abundant following therapy.

384 Patients often deteriorate rapidly once treatment resistance develops and having an early signal
385 could significantly change treatment by accelerating testing of new drugs, or drug-radiation
386 combinations. Collectively, our GEMPAC platform opens a window for monitoring brain
387 pathologies during therapy and offers a unique view of changes in the GBM sEV landscape at
388 various stages of disease evolution. This assay has potential broad clinical implications and could
389 be utilized to not only predict treatment outcomes, but also determine the phenotypic heterogeneity
390 of GBM. The capability of monitoring the emergence of specific GSCs associated with distinct
391 GBM cellular states might be therapeutically important as targeted elimination of specific GSCs
392 might have clinical benefit. As a result, we envisage with future validation in larger clinical
393 cohorts, the high sensitivity of our GEMPAC platform could be utilized for predicting optimal
394 treatment approaches in new areas of therapeutic development for GBM patients.

395 **MATERIALS AND METHODS**

396 **Clinical sample acquisition**

397 This study was approved by the Human Research Ethics Committee of the University of Newcastle
398 (H-2020-0231). Informed consent was received from all patients. Blood was obtained from non-
399 fasted patients before surgery, post-surgery (1-7 days) and at the time of treatment in EDTA-coated
400 tubes. Whole blood was centrifuged twice to deplete platelets and separate plasma. Plasma was
401 then aliquoted and stored at -80°C until use. Formalin-fixed paraffin-embedded tumor tissue from
402 surgical resection was sourced from the Mark Hughes Foundation Brain Bank facilitated by the
403 NSW Regional Biospecimen Services for 36 cases of glioblastoma (Supplementary, Table S1). A
404 block containing maximal tumor content was chosen from each patient and diagnosis of
405 glioblastoma confirmed on H&E sections by a neuropathologist (Dr. Ricardo Vilain, Hunter Area
406 Health Service). Clinical information is available in Supplementary, Table S1 including age,
407 gender, treatment information, *MGMT* promoter methylation status, overall survival information,
408 isocitrate dehydrogenase (IDH) status, EGFR status, glial fibrillary acidic protein (GFAP) status,
409 and alpha-thalassemia/mental retardation, X-linked (ATRX) status.

410 **Bioinformatic analysis to identify brain specific surface proteins**

411 Our objective was to identify robust brain-specific markers for the capture of CNS-specific sEVs.
412 We conducted a bioinformatic analysis to select CNS-specific markers based on data sourced from
413 The Cancer Genome Atlas (TCGA), the Genotype-Tissue Expression (GTEx), and the UniProt
414 database as previously described.[61] This integration enabled a comprehensive investigation of
415 markers specific to the brain. Subsequently, we utilized The Human Protein Atlas, to refine the
416 selection of markers with an extracellular domain and selected candidates with medium to strong
417 immunohistochemistry staining. Following this, the surface markers ATP1B2 and EAAT2 were
418 selected based on the availability of suitable antibodies that target the extracellular domain of each
419 protein.

420 **Cell culture**

421 Primary patient-derived Q-Cell GBM cell lines were obtained under MTA from QIMR Berghofer
422 Medical Research Institute.[49, 62, 63] BAH1 (QIMR-B001), WK1 (QIMR-B012), and FPW1
423 (QIMR-B002) were cultured in serum-free KnockOut™ DMEM/F-12 medium supplemented with
424 StemPro® neural supplement (Thermo Fisher Scientific), epidermal growth factor (EGF) (20
425 ng/mL), and fibroblast growth factor (FGF) (10 ng/mL) (StemPro™ NSC SFM). Cells were
426 maintained as an adherent monolayer on a basement membrane of Matrigel (Corning).[49] For
427 sEV isolation, BAH1, WK1, and FPW1 cells were cultured using Cytodex-1 microcarriers.

428 **Preparation of microcarriers**

429 Cytodex-1 microcarriers (Cytiva) were prepared according to the manufacturer's guidelines.
430 Briefly, dry Cytodex-1 microcarriers were hydrated with PBS (50 ml/g Cytodex-1) for at least 4
431 hours and washed 2 times with the same volume of PBS before being autoclaved (121 °C, 15 psi
432 for 30 mins). Microcarriers were then coated with Matrigel (1:30) before being washed and
433 equilibrated in StemPro™ NSC SFM.

434 **Cell line sEV medium collection**

435 BAH1, WK1, and FPW1 cells were seeded at 2×10^5 cells/mL containing 2 g/L of Cytodex-1
436 microcarriers in 1/3 of the final volume of StemPro™ NSC SFM with periodic stirring at 37 °C
437 for 3 hours. After 3 hours, the volume of the culture was increased to the final volume and
438 continuous shaking commenced at 90 RPM to keep the microcarriers in suspension. Cells were
439 cultured for 72 hours before the culture medium was collected and centrifuged at $500 \times g$ for 10
440 min and then filtered through a 0.22 µm filter to remove cell debris and large EVs. The filtered
441 culture media was then concentrated using tangential flow filtration as previously described in
442 detail.[64] Briefly, media was prepared for sEV purification by concentrating with a sterile
443 Minimate 300kDa Omega Membrane (Pall Corporation) Tangential Flow Filtration Capsule to
444 approximately 20 mL with continuous diafiltration (5 diafiltration volumes), and further
445 concentrated with a Centricon Plus-70 100 kDa (Merck) to approximately 500 µL before being
446 purified with SEC.

447 **sEV purification**

448 sEVs were purified from GBM cell culture medium and patient plasma samples using SEC as
449 previously described in detail.[50, 64] Patient plasma samples was thawed from -80°C and kept
450 on ice. Aliquots of 500 µL were centrifuged at $10,000 \times g$ for 10 minutes at 4°C to pellet any
451 remaining cellular debris or larger particles. Concentrated culture medium or clarified patient
452 samples were subsequently applied to Izon qEV Original 70 nm columns (Izon Science) and eluted
453 in filtered phosphate-buffered saline (PBS, Sigma-Aldrich). Following the void volume, the
454 following 1.6 mL of sEV-enriched fractions were concentrated to $\leq 50 \mu\text{L}$ using Amicon Ultra-4
455 10 kDa MWCO columns (Merck) at $3,500 \times g$ for approximately 45 minutes at 4°C. The
456 concentrated sEV isolates were aliquoted and stored at -80°C.

457 **Nanoparticle tracking analysis (NTA)**

458 NanoSight N300 (NanoSight Nanoparticle Tracking and Analysis Release Version Build 3.4) was
459 used as previously published [64]. Briefly, the samples were diluted with PBS to a particle range
460 of 50 – 100 particles per frame. Samples were analyzed at 25°C. The camera level was set to
461 provide sufficient contrast to identify particles while minimizing background noise and samples
462 were recorded in triplicate.

463 **Measurement of sEV Size and Concentration using nanoFCM**

464 Purified sEV samples were analyzed by nanoFCM equipped with 488 and 640 nm
465 lasers. Concentration and fluorescence measurements were calibrated with 250 nm silica
466 nanospheres labelled with fluorochromes at 20 mW laser power, 0.2% SS decay and 1 kPa
467 sampling pressure. The particle size distribution of sEVs was calibrated at 10 mW laser power,
468 10% SS decay and 1 kPa sampling pressure using a four-modal standard silica nanoparticle
469 cocktail (68~155 nm) which has a similar refractive index to EVs.[65] Positive particles were gated
470 based on a negative control of PBS or the respective fluorescent antibody to adjust for background
471 fluorescence

472 **sEV immunofluorescent staining for nanoFCM**

473 Approximately 1×10^9 total sEV particles were incubated with either anti-ATP1B2 (PA526279,
474 Thermo Fisher Scientific), anti-EAAT2 (NOVNB120136, Novus), anti-CD9 APC (17-0098-42,

475 Thermo Fisher Scientific), anti-CD24 (ab134375, Abcam), anti-EGFR (ab231, Abcam), anti-
476 CD44 Alexa Fluor 488 (103016, BioLegend), or anti-CD133 Alexa Fluor 488 (FAB11331G, R&D
477 Systems) in 50 μ L of PBS, for 1 h at 37 °C. Labeled sEVs were diluted with 1 mL of PBS and
478 ultracentrifuged at 110,000 \times g for 30 min using an Optima MAX-XP Benchtop Ultracentrifuge
479 (Beckman-Coulter) TLA-100.3 rotor (k-Factor 14). Samples labeled with anti-ATP1B2 and anti-
480 EAAT2, anti-EGFR, and anti-CD24 were subsequently incubated with goat anti-rabbit IgG H&L
481 APC (ab130805, Abcam), anti-rat IgG2a heavy chain Alexa Fluor 488 (ab172332, Abcam), and
482 anti-mouse IgG Alexa Fluor 488 (ab150113, Abcam) respectively for 1 h at 37 °C, and
483 ultracentrifuged as before. The supernatant was removed and the sEV pellet was resuspended in
484 50 μ L of filtered PBS for analysis with the nanoFCM equipped with 488 and 640 nm lasers. Data
485 was analyzed using FlowJo version 10.8.1.

486 **Western blot**

487 GBM patient-derived cells (BAH1, WK1, and FPW1) and their sEVs were reduced and denatured
488 by Laemmli buffer and 2-mercaptoethanol (Bio-Rad) for 5 minutes at 95°C. Proteins were resolved
489 by SDS-polyacrylamide gel electrophoresis (SDS-PAGE) and then transferred to polyvinylidene
490 fluoride membranes (Bio-Rad). The membranes were blocked with 5% skim milk in PBS-T (0.1%
491 Tween-20) for 30 minutes at room temperature (RT). Primary antibodies, anti-Calnexin (2679,
492 Cell Signaling) and anti-Hsp70 (610608, BD Biosciences), were applied at the recommended
493 dilutions for 1 hour of incubation at RT. After incubation, the membranes were washed five times
494 with PBS-T and incubated with a HRP-conjugated secondary antibody for 1 hour at RT. The
495 membranes were then washed five times with PBS-T and visualized using enhanced
496 chemiluminescence reagent (Clarity Western ECL Substrate, Bio-Rad) and the Bio-Rad
497 ChemiDoc Imaging System.

498 **TEM**

499 For TEM analysis, 2.5 μ L of isolated sEVs (1×10^{11} particles/mL) were fixed with an equal volume
500 of 2% glutaraldehyde for 30 minutes at RT. Subsequently, 5 μ L of fixed sample was loaded on
501 Formvar/carbon-coated electron microscopic grids (Electron Microscopy Science) and incubated
502 for 15 minutes and excess liquid was removed by blotting. The grid was washed three times by

503 brief contact with 100 μL of Milli-Q water, followed by blotting to remove excess liquid. To
504 contrast the sample, the grid was negatively stained with 30 μL of 2% uranyl acetate (w/v) for 5
505 minutes and excess fluid was removed by blotting gently. Grids were left to air dry and observed
506 using transmission electron microscopy (Hitachi HT7700) at 100 kV.

507 **GEMPAC Chip fabrication**

508 The GEMPAC device with 28 asymmetric electrodes was fabricated with standard
509 photolithography as previously reported.[66, 67] The electrode pattern was designed using Layout
510 Editor L-Edit V15 (Tanner Research) and written on 5-inch soda lime chrome masks (Shenzhen
511 Qingyi Precision Mask Making) using a direct write system μPG 101 (Heidelberg Instruments).
512 Then, a clean 4-inch Boroflat wafer (Bonda Technology Pte Ltd) was spin-coated with a negative
513 photoresist AZnLOF 2020 (Microchemicals GmbH) at 3000 rpm for 30 seconds. After a soft bake
514 for 2 minutes at 110 $^{\circ}\text{C}$, the wafer was UV-exposed with the above prepared mask at a constant
515 dose of 200 mJ cm^{-1} using a mask aligner (EVG 620, EV Group, St Florian am Inn), following a
516 post-exposure bake for 1 minute at 110 $^{\circ}\text{C}$ and wafer development for 30 s using an AZ726 MIF
517 Developer (Microchemicals GmbH). The gold electrodes were then created by deposition of 10
518 nm Titanium and 200 nm gold using a Temescal FC-2000 Deposition System (Ferrotec) and
519 overnight lift-off in Remover PG (Microchemicals GmbH). The wafer carrying the gold electrode
520 structures was rinsed with isopropanol and dried under a flow of nitrogen.

521 To accommodate the liquid sample analysis, a 4 mm-thick polydimethylsiloxane (PDMS) slab
522 with microfluidic well structures was manually aligned to electrodes of the device. The PDMS
523 slab was prepared by curing activated silicon elastomer solution (Sylgard 184, Dow) for 2 h at 65
524 $^{\circ}\text{C}$. The PDMS slab was then punched with 5 mm-diameter wells and thermally bonded to the
525 device overnight at 65 $^{\circ}\text{C}$.

526 **SERS nanotag synthesis and functionalization**

527 60 nm gold nanoparticles were synthesized through citrate reduction of gold (III) chloride
528 trihydrate (HAuCl_4 , Sigma-Aldrich).[68] 0.01% (w/v) of HAuCl_4 was added into 100 mL Milli-Q
529 water and heated till boiling. 1 mL of 1% (w/v) of trisodium citrate dehydrate (Univar Solutions)
530 was quickly added into the boiling solution with constant mixing and kept at a boil for 20 minutes

531 with constant mixing. To synthesize SERS nanotags, 1 mL of gold nanoparticle solution was
532 incubated with 2 μ L of 1 mM Dithiobis (succinimidyl pro) (DSP, Thermo Fisher Scientific) and
533 10 μ L of a 1 mM Raman reporter (Sigma-Aldrich) for 5-7 h with gentle shaking (350 rpm) at RT.
534 After that, the solution was centrifuged at 5400 $\times g$ for 10 min and resuspend in 200 μ L of 0.1 mM
535 PBS buffer. The Raman intensity for each SERS nanotag was measured. After that, the solution
536 was then incubated with 1 μ g of paired antibodies, anti-ATP1B2 (PA526279, Thermo Fisher
537 Scientific), anti-EAAT2 (NOVNBP120136, Novus Biologicals), anti-CD24 (ab134375, Abcam),
538 anti-EGFR (ab231, Abcam), anti-CD133 (130108062, Miltenyi Biotec) and anti-CD44
539 (14044182, Thermo Fisher Scientific) for 30 minutes at RT. The solution was then centrifuged at
540 600 $\times g$ for 6 minutes to remove excess antibodies. After that, SERS nanotags were resuspended
541 in 0.1% (w/v) bovine serum albumin (BSA) to block non-specific binding. The patterns of Raman
542 reporters with antibodies were DTNB-ATP1B2, MBA-EAAT2, TFMBA-CD44, and MPY-
543 CD133.

544 **GEMPAC functionalization and operation**

545 20 μ L of 5 mM DSP were incubated at the center circular electrode for 30 min at RT. Following
546 this, electrodes were washed once with absolute EtOH followed by 3 washes of 1 \times PBS. Next, 20
547 μ L of 10 μ g/mL of capture antibodies for 2 h at RT were incubated on the electrode. The electrode
548 was then blocked with 5% (w/v) BSA in PBS and incubated overnight at 4 $^{\circ}$ C. After blocking,
549 electrodes were washed 3 times with 1% (w/v) BSA in PBS before sample addition. A total of 5 \times
550 10⁸ sEVs in 50 μ L was added into the circular electrode and an alternative current field of 800 mV
551 and 599 Hz was applied for 45 minutes. Electrodes were then washed 3 times with 1% (w/v) BSA
552 in PBS before the addition of 20 μ L of SERS nanotags (1 in 25 dilutions in 1% (w/v) BSA in PBS).
553 The electric field with same conditions as above was carried out for 20 min. Electrodes were then
554 finally washed 3 times with 1% (w/v) BSA in PBS.

555 **SERS mapping and analysis**

556 Samples were analyzed and recorded by Witec alpha 300 R micro-spectrometer using a 632.8 nm
557 excitation wavelength from a HeNe laser (laser power 4 mW). The integration time for
558 measurement is 0.05 s on each electrode. Each sample has 2-3 separate electrodes as technique

559 replicates. Each electrode was measured with two areas of $60\ \mu\text{m} \times 60\ \mu\text{m}$ (60 pixels \times 60 pixels)
560 squares using a $20\times$ objective. The signal peak was based on each Raman reporter's signature
561 peak, MPY – $1000\ \text{cm}^{-1}$, MBA – $1078\ \text{cm}^{-1}$, DTNB – $1333\ \text{cm}^{-1}$, and TFMBA – $1378\ \text{cm}^{-1}$. The
562 signal intensity was calculated and representative of each protein marker's expression level on
563 sEVs.

564 **Immunohistochemistry**

565 Formalin-fixed paraffin-embedded tumor tissue was sliced into $4\ \mu\text{m}$ full face sections and
566 processed for 3',3'-diaminobenzidine (DAB) immunohistochemistry using a Ventana Discovery
567 Ultra (Roche) by the HCB. 31 out of 32 patients' tissues were available for IHC staining. Sections
568 were labeled with rabbit antibodies directed at either EAAT2 ATP1B2, EGFR, CD133 and CD44
569 (Supplementary, Table S2). All steps, from baking to chromogen addition were performed
570 automatically by the instrument. Tissue sections were baked to slides and deparaffinized, and
571 antigen retrieval then occurred at $95\ ^\circ\text{C}$ / pH 9 with a total incubation time of 24 minutes before
572 the addition of the primary antibody. The addition of the primary antibody was followed by a 32-
573 minute incubation at $36\ ^\circ\text{C}$. Slides were then incubated with a secondary antibody – Anti-Rabbit
574 HQ (Roche), for 20 minutes at $36\ ^\circ\text{C}$. Positive control and negative control tissues were included
575 in each batch of slides to confirm the specificity of antibody labeling.

576 **Quantitative IHC analyses**

577 GBM tissue slides were digitally scanned using the Aperio™ Digital AT2 Pathology System
578 (Leica Biosystems) at $40\times$ absolute resolution. Quantitative IHC analyses were performed using
579 the HALO™ image analysis platform (version 3.0, Indica Labs, NM). Tissue classification
580 algorithms were used to differentiate tissue regions, such as tumors, necrosis, adjacent normal
581 brain, followed by quantification of pixel intensity values corresponding to DAB staining of
582 protein biomarkers. Area quantification algorithm, which detects biomarker expression across the
583 whole tumor, as well as the cytonuclear algorithm, which quantifies based on cellular
584 compartment, were both used dependent on protein biomarker localization. The labeling intensity
585 of each marker was measured across four representative areas of each tumor and average H-scores
586 for each biomarker for each tumor was calculated as: $\text{H-score} = (1 \times \% \text{ weak positive tissue}) + (2$

587 x % moderate positive tissue) + (3 x % strong positive tissue) with a range of 0 - 300. H-scores
588 were then used to create distribution plots to show biomarker intensity across the cohort of
589 glioblastoma cases.

590 **Normalization of GSC markers and GEMPAC score**

591 CD44, CD133, EGFR and CD24 were normalized by the sum of CNS markers ATP1B2 and
592 EAAT2 at each time point to investigate changes in relative GSC marker expression. To track the
593 abundance of GBM sEVs in circulation, the GEMPAC score is equal to the sum of normalized all
594 GSC markers.

$$595 \quad (1) \text{ Normalized GSC expression} = \frac{\text{GSC marker}}{\text{sum(ATP1B2 + EAAT2)}}$$

596 (2) GEMPAC score

597 = Normalized CD24 + Normalized EGFR + Normalized CD44

598 + Normalized CD133

599 **Statistical analysis**

600 No statistical methods were used to predetermine sample size. All statistical analyses were
601 performed using GraphPad Prism (GraphPad Software v.10.1.2) and values are given as
602 mean ± sem or sd as indicated. When two groups were compared, significance was determined
603 using an unpaired two-tailed t-test. A log-rank test was used to assess significance in Kaplan–
604 Meier survival analysis. One-way ANOVA, or Two-way ANOVA were used for multiple
605 comparisons, and P values adjusted using Tukey, or Šidák for multiple comparisons where it was
606 appropriate. P value threshold of 0.05 was considered statistically significant.

607 **List of Supplementary Materials**

608 Fig. S1 to S14 for multiple supplementary figures

609 Table S1 to S2 for multiple supplementary tables

610 **Acknowledgments**

611 The authors acknowledge the staff of the NSW Regional Biospecimen Services, University of
612 Newcastle for sourcing the glioblastoma tumor tissue, bloods and clinical data from the Mark
613 Hughes Foundation Biobank and for completing the immunohistochemistry. We also acknowledge
614 the staff from the Histology Facility at the Hunter Medical Research Institute for cutting the tissue
615 blocks and scanning all the slides. We thank the Mark Hughes Foundation for providing funding
616 for the Biobank and for directly funding this work. X.N. acknowledges the China Scholarship
617 Council (CSC) scholarship.

618 **Author contributions:** Z.Z., R.J.L., designed and performed experiments, analyzed and interpreted
619 the data, and directed the research. R.L., S.F., P.T., and M.F. were involved in patient sample
620 analysis. Q.Z., was involved in fabrication and chip design. X.N. was involved in EV
621 characterization. B.W.D. contributed patient-derived GBM cell lines and supervised cell line
622 study. Z.Z., R.J.L., J.W., S.P., S.R., P.T., and M.T. conceived the study and initiated the research.
623 All authors discussed the results and participated in writing, and revising the manuscript, and
624 approved the submitted version.

625 **Competing interests:** The authors declare no competing interests.

626 **Data and materials availability:** The data that support the findings of this study are available
627 from the corresponding author upon reasonable request.

References

- 628 1. Cloughesy, T.F., W.K. Cavenee, and P.S. Mischel, *Glioblastoma: From Molecular*
629 *Pathology to Targeted Treatment*. Annual Review of Pathology: Mechanisms of Disease,
630 2014. **9**(1), 1-25
- 631 2. Saadatpour, L., et al., *Glioblastoma: exosome and microRNA as novel diagnosis*
632 *biomarkers*. Cancer Gene Therapy, 2016. **23**(12), 415-418
- 633 3. Tan, A.C., et al., *Management of glioblastoma: State of the art and future directions*. CA:
634 A Cancer Journal for Clinicians, 2020. **70**(4), 299-312
- 635 4. de la Iglesia, N., S.V. Puram, and A. Bonni, *STAT3 regulation of glioblastoma*
636 *pathogenesis*. Current Molecular Medicine, 2009. **9**(5), 580-90
- 637 5. Hanif, F., et al., *Glioblastoma Multiforme: A Review of its Epidemiology and Pathogenesis*
638 *through Clinical Presentation and Treatment*. Asian Pacific Journal of Cancer Prevention,
639 2017. **18**(1), 3-9
- 640 6. Huang, R.Y., et al., *Pitfalls in the neuroimaging of glioblastoma in the Era of*
641 *antiangiogenic and immuno/targeted therapy – detecting illusive disease, defining*
642 *response*. Frontiers in Neurology, 2015. **6**, 33
- 643 7. Müller Bark, J., et al., *Circulating biomarkers in patients with glioblastoma*. British Journal
644 of Cancer, 2020. **122**(3), 295-305
- 645 8. Zikou, A., et al., *Radiation necrosis, pseudoprogression, pseudoresponse, and tumor*
646 *recurrence: imaging challenges for the evaluation of treated gliomas*. Contrast Media &
647 Molecular Imaging, 2018. **2018**, 6828396-6828396
- 648 9. Sharma, A. and R. Kumar, *Metabolic Imaging of Brain Tumor Recurrence*. AJR. American
649 Journal of Roentgenology, 2020. **215**(5), 1199-1207
- 650 10. Shankar, G.M., et al., *Liquid biopsy for brain tumors*. Expert Review of Molecular
651 Diagnostics, 2017. **17**(10), 943-947
- 652 11. Perakis, S. and M.R. Speicher, *Emerging concepts in liquid biopsies*. BMC Medicine,
653 2017. **15**(1), 75
- 654 12. An, Y., et al., *Recent Advances in Liquid Biopsy of Brain Cancers*. Frontiers in Genetics,
655 2021. **12**, 720270
- 656 13. Möller, A. and R.J. Lobb, *The evolving translational potential of small extracellular*
657 *vesicles in cancer*. Nature Reviews Cancer, 2020. **20**(12), 697-709
- 658 14. Onukwugha, N.E., Y.T. Kang, and S. Nagrath, *Emerging micro-nanotechnologies for*
659 *extracellular vesicles in immuno-oncology: from target specific isolations to*
660 *immunomodulation*. Lab Chip, 2022. **22**(18), 3314-3339
- 661 15. Gourlay, J., et al., *The emergent role of exosomes in glioma*. Journal of Clinical
662 Neuroscience, 2017. **35**, 13-23
- 663 16. Soung, Y., et al., *Exosomes in Cancer Diagnostics*. Cancers, 2017. **9**(12), 8
- 664 17. Al-Nedawi, K., et al., *Intercellular transfer of the oncogenic receptor EGFRvIII by*
665 *microvesicles derived from tumour cells*. Nature Cell Biology, 2008. **10**(5), 619-24

- 666 18. García-Romero, N., et al., *DNA sequences within glioma-derived extracellular vesicles can*
667 *cross the intact blood-brain barrier and be detected in peripheral blood of patients.*
668 *Oncotarget*, 2017. **8**(1), 1416-1428
- 669 19. Osti, D., et al., *Clinical Significance of Extracellular Vesicles in Plasma from Glioblastoma*
670 *Patients.* *Clinical Cancer Research*, 2019. **25**(1), 266-276
- 671 20. Sabbagh, Q., et al., *The von Willebrand factor stamps plasmatic extracellular vesicles from*
672 *glioblastoma patients.* *Scientific Reports*, 2021. **11**(1), 22792
- 673 21. Johnsen, K.B., et al., *What is the blood concentration of extracellular vesicles?*
674 *Implications for the use of extracellular vesicles as blood-borne biomarkers of cancer.*
675 *Biochimica et Biophysica Acta (BBA) - Reviews on Cancer*, 2019. **1871**(1), 109-116
- 676 22. Kuravi, S.J., et al., *Changes in the pattern of plasma extracellular vesicles after severe*
677 *trauma.* *PLOS ONE*, 2017. **12**(8), e0183640
- 678 23. Figueroa, J.M., et al., *Detection of wild-type EGFR amplification and EGFRvIII mutation*
679 *in CSF-derived extracellular vesicles of glioblastoma patients.* *Neuro-Oncology*, 2017.
680 **19**(11), 1494-1502
- 681 24. Gomes, D.E. and K.W. Witwer, *LICAM-associated extracellular vesicles: A systematic*
682 *review of nomenclature, sources, separation, and characterization.* *Journal of*
683 *Extracellular Biology*, 2022. **1**(3), e35
- 684 25. Indira Chandran, V., et al., *Ultrasensitive Immunoprofiling of Plasma Extracellular*
685 *Vesicles Identifies Syndecan-1 as a Potential Tool for Minimally Invasive Diagnosis of*
686 *Glioma.* *Clinical Cancer Research*, 2019. **25**(10), 3115-3127
- 687 26. Mojiri, A., et al., *Functional assessment of von Willebrand factor expression by cancer*
688 *cells of non-endothelial origin.* *Oncotarget*, 2017. **8**(8), 13015-13029
- 689 27. Teng, Y.H., R.S. Aquino, and P.W. Park, *Molecular functions of syndecan-1 in disease.*
690 *Matrix Biology*, 2012. **31**(1), 3-16
- 691 28. Li, S., et al., *Targeting $\beta 2$ subunit of Na(+)/K(+)-ATPase induces glioblastoma cell*
692 *apoptosis through elevation of intracellular Ca(2).* *American Journal of Cancer Research*,
693 2019. **9**(6), 1293-1308
- 694 29. Sun, M.Z., et al., *Na⁺/K⁺-ATPase $\beta 2$ -subunit (AMOG) expression abrogates invasion of*
695 *glioblastoma-derived brain tumor-initiating cells.* *Neuro-Oncology*, 2013. **15**(11), 1518-
696 31
- 697 30. Corbetta, C., et al., *Altered function of the glutamate-aspartate transporter GLAST, a*
698 *potential therapeutic target in glioblastoma.* *International Journal of Cancer*, 2019.
699 **144**(10), 2539-2554
- 700 31. Suva, M.L. and I. Tirosh, *The Glioma Stem Cell Model in the Era of Single-Cell Genomics.*
701 *Cancer Cell*, 2020. **37**(5), 630-636
- 702 32. Filbin, M.G., et al., *Developmental and oncogenic programs in H3K27M gliomas dissected*
703 *by single-cell RNA-seq.* *Science*, 2018. **360**(6386), 331-335
- 704 33. Tirosh, I., et al., *Single-cell RNA-seq supports a developmental hierarchy in human*
705 *oligodendroglioma.* *Nature*, 2016. **539**(7628), 309-313

- 706 34. Wuethrich, A., et al., *Interfacial nano-mixing in a miniaturised platform enables signal*
707 *enhancement and in situ detection of cancer biomarkers*. *Nanoscale*, 2018. **10**(23), 10884-
708 10890
- 709 35. Robert, S.M. and H. Sontheimer, *Glutamate transporters in the biology of malignant*
710 *gliomas*. *Cellular and Molecular Life Sciences : CMLS*, 2014. **71**(10), 1839-1854
- 711 36. Alam, M.A. and P.K. Datta, *Epigenetic Regulation of Excitatory Amino Acid Transporter*
712 *2 in Neurological Disorders*. *Frontiers in Pharmacology*, 2019. **10**, 483008
- 713 37. Shao, H., et al., *Chip-based analysis of exosomal mRNA mediating drug resistance in*
714 *glioblastoma*. *Nature Communications*, 2015. **6**, 6999
- 715 38. Vaillant, B.D., et al., *CD44 as a prognostic and predictive marker for GBM*. *Journal of*
716 *Clinical Oncology*, 2011. **29**(15_suppl), 2049-2049
- 717 39. Couturier, C.P., et al., *Single-cell RNA-seq reveals that glioblastoma recapitulates a*
718 *normal neurodevelopmental hierarchy*. *Nature Communications*, 2020. **11**(1), 3406
- 719 40. Soni, P., et al., *CD24 and Nanog expression in Stem Cells in Glioblastoma: Correlation*
720 *with Response to Chemoradiation and Overall Survival*. *Asian Pacific Journal of Cancer*
721 *Prevention*, 2017. **18**(8), 2215-2219
- 722 41. Senner, V., et al., *CD24 promotes invasion of glioma cells in vivo*. *Journal of*
723 *Neuropathology & Experimental Neurology*, 1999. **58**(8), 795-802
- 724 42. Hatanpaa, K.J., et al., *Epidermal growth factor receptor in glioma: signal transduction,*
725 *neuropathology, imaging, and radioresistance*. *Neoplasia*, 2010. **12**(9), 675-84
- 726 43. Brown, D.V., et al., *Expression of CD133 and CD44 in glioblastoma stem cells correlates*
727 *with cell proliferation, phenotype stability and intra-tumor heterogeneity*. *PLOS ONE*,
728 2017. **12**(2), e0172791
- 729 44. Si, D., et al., *High Expression of CD44 Predicts a Poor Prognosis in Glioblastomas*.
730 *Cancer Management and Research*, 2020. **12**, 769-775
- 731 45. Ahmed, S.I., et al., *CD133 Expression in Glioblastoma Multiforme: A Literature Review*.
732 *Cureus*, 2018. **10**(10), e3439
- 733 46. Liou, G.Y., *CD133 as a regulator of cancer metastasis through the cancer stem cells*. *The*
734 *International Journal of Biochemistry & Cell Biology*, 2019. **106**, 1-7
- 735 47. Prager, B.C., et al., *Glioblastoma Stem Cells: Driving Resilience through Chaos*. *Trends*
736 *in Cancer*, 2020. **6**(3), 223-235
- 737 48. Bhaduri, A., et al., *Outer Radial Glia-like Cancer Stem Cells Contribute to Heterogeneity*
738 *of Glioblastoma*. *Cell Stem Cell*, 2020. **26**(1), 48-63.e6
- 739 49. Stringer, B.W., et al., *A reference collection of patient-derived cell line and xenograft*
740 *models of proneural, classical and mesenchymal glioblastoma*. *Scientific Reports*, 2019.
741 **9**(1), 4902
- 742 50. Lobb, R.J., et al., *Optimized exosome isolation protocol for cell culture supernatant and*
743 *human plasma*. *Journal of Extracellular Vesicles*, 2015. **4**(1), 27031

- 744 51. Grabowski, M.M., et al., *Residual tumor volume versus extent of resection: predictors of*
745 *survival after surgery for glioblastoma*. *Journal of Neurosurgery*, 2014. **121**(5), 1115-23
- 746 52. Abdoli Shadbad, M., et al., *The Prognostic Value of CD133 in Predicting the Relapse and*
747 *Recurrence Pattern of High-Grade Gliomas on MRI: A Meta-Analysis*. *Frontiers in*
748 *Oncology*, 2021. **11**, 722833
- 749 53. Behnan, J., G. Finocchiaro, and G. Hanna, *The landscape of the mesenchymal signature in*
750 *brain tumours*. *Brain*, 2019. **142**(4), 847-866
- 751 54. De Silva, M.I., B.W. Stringer, and C. Bardy, *Neuronal and tumourigenic boundaries of*
752 *glioblastoma plasticity*. *Trends in Cancer*, 2023. **9**(3), 223-236
- 753 55. Kim, Y., et al., *Perspective of mesenchymal transformation in glioblastoma*. *Acta*
754 *Neuropathologica Communications*, 2021. **9**(1), 50
- 755 56. Halliday, J., et al., *In vivo radiation response of proneural glioma characterized by*
756 *protective p53 transcriptional program and proneural-mesenchymal shift*. *Proceedings of*
757 *the National Academy of Sciences*, 2014. **111**(14), 5248-5253
- 758 57. Wang, L., et al., *A single-cell atlas of glioblastoma evolution under therapy reveals cell-*
759 *intrinsic and cell-extrinsic therapeutic targets*. *Nature Cancer*, 2022. **3**(12), 1534-1552
- 760 58. Genoud, V., et al., *Therapeutic Targeting of Glioblastoma and the Interactions with Its*
761 *Microenvironment*. *Cancers (Basel)*, 2023. **15**(24), 5790
- 762 59. Lakis, N.S., et al., *Stem cell phenotype predicts therapeutic response in glioblastomas with*
763 *MGMT promoter methylation*. *Acta Neuropathologica Communications*, 2022. **10**(1), 159
- 764 60. Fedele, M., et al., *Proneural-Mesenchymal Transition: Phenotypic Plasticity to Acquire*
765 *Multitherapy Resistance in Glioblastoma*. *International Journal of Molecular Sciences*,
766 2019. **20**(11), 2746
- 767 61. Zaborowski, M.P., et al., *Methods for Systematic Identification of Membrane Proteins for*
768 *Specific Capture of Cancer-Derived Extracellular Vesicles*. *Cell Reports*, 2019. **27**(1), 255-
769 268 e6
- 770 62. D'Souza, R.C.J., et al., *Q-Cell Glioblastoma Resource: Proteomics Analysis Reveals*
771 *Unique Cell-States are Maintained in 3D Culture*. *Cells*, 2020. **9**(2), 267
- 772 63. Day, B.W., et al., *Glioma surgical aspirate: a viable source of tumor tissue for*
773 *experimental research*. *Cancers (Basel)*, 2013. **5**(2), 357-71
- 774 64. Visan, K.S., et al., *Comparative analysis of tangential flow filtration and*
775 *ultracentrifugation, both combined with subsequent size exclusion chromatography, for the*
776 *isolation of small extracellular vesicles*. *Journal of Extracellular Vesicles*, 2022. **11**(9),
777 12266
- 778 65. Welsh, J.A., et al., *Towards defining reference materials for measuring extracellular*
779 *vesicle refractive index, epitope abundance, size and concentration*. *Journal of*
780 *Extracellular Vesicles*, 2020. **9**(1), 1816641
- 781 66. Wuethrich, A., et al., *Single droplet detection of immune checkpoints on a multiplexed*
782 *electrohydrodynamic biosensor*. *Analyst*, 2019. **144**(23), 6914-6921

- 783 67. Zhang, Z., et al., *Tracking Drug-Induced Epithelial–Mesenchymal Transition in Breast*
784 *Cancer by a Microfluidic Surface-Enhanced Raman Spectroscopy Immunoassay*. *Small*,
785 2020. **16**(13), 1905614
- 786 68. Frens, G., *Controlled nucleation for the regulation of the particle size in monodisperse*
787 *gold suspensions*. *Nature Physical Science*, 1973. **241**(105), 20-22